International Journal of Nanomedicine

Dovepress
open access to scientific and medical research

Open Access Full Text Article

ORIGINAL RESEARCH

Smart Chondroitin Sulfate Micelles for Effective Targeted Delivery of Doxorubicin Against Breast Cancer Metastasis

Jingmou Yu[1,2], Xin Xie[2], Liangliang Wang[3], Wenbo Liu[4], Huifeng Xu[4], Xiangmei Lu[4], Xiaofan Li[4], Jin Ren[2,4], Weidong Li[2,5]

[1]Huzhou Key Laboratory of Medical and Environmental Applications Technologies, School of Life Sciences, Huzhou University, Huzhou, 313000, People's Republic of China; [2]Jiangxi Provincial Key Laboratory of System Biomedicine, Jiujiang University, Jiujiang, 332000, People's Republic of China; [3]Affiliated Hospital of Jiujiang University, Jiujiang, 332000, People's Republic of China; [4]School of Pharmacy and Life Sciences, Jiujiang University, Jiujiang, 332000, People's Republic of China; [5]Jiujiang NO.1 People's Hospital & Water of Life Hospital, Jiujiang, 332000, People's Republic of China

Correspondence: Jin Ren; Weidong Li, Email yanjiushengrj@126.com; 346880908@qq.com

International Journal of Nanomedicine downloaded from https://www.dovepress.com/
For personal use only.

Introduction: Metastasis is a major challenge in breast cancer therapy. The successful chemotherapy of breast cancer largely depends on the ability to block the metastatic process. Herein, we designed a dual-targeting and stimuli-responsive drug delivery system for targeted drug delivery against breast cancer metastasis.

Methods: AS1411 aptamer-modified chondroitin sulfate A-ss-deoxycholic acid (ACSSD) was synthesized, and the unmodified CSSD was used as the control. Chemotherapeutic drug doxorubicin (DOX)-containing ACSSD (D-ACSSD) micelles were prepared by a dialysis method. The ACSSD conjugate was confirmed by Fourier transform infrared spectroscopy (FTIR), nuclear magnetic resonance (NMR), dynamic light scattering (DLS), and transmission electron microscopy (TEM). In vitro cellular uptake and cytotoxicity of D-ACSSD micelles were studied by confocal laser scanning microscopy (CLSM) and MTT assay in breast tumor cells. The inhibition capability of D-ACSSD micelles in cell migration and invasion was carried out in 4T1 cells. In vivo antitumor activity of DOX-containing micelles was investigated in metastatic 4T1-bearing Balb/c mice.

Results: D-ACSSD and DOX-loaded CSSD (D-CSSD) micelles exhibited high drug encapsulation content and reduction-responsive characteristics. D-ACSSD micelles were spherical in shape. Compared with D-CSSD, D-ACSSD showed higher cellular uptake and more potent killing activity in 4T1 and MDA-MB-231 cells. Additionally, D-ACSSD exhibited stronger inhibitory effects on the invasion and migration of highly metastatic 4T1 cells than unmodified D-CSSD. Among the DOX-containing formulations, D-ACSSD micelles presented the most effective inhibition of tumor growth and lung metastasis in orthotopic 4T1-bearing mice in vivo. It also revealed that ACSSD micelles did not exhibit obvious systemic toxicity.

Conclusion: The smart D-ACSSD micelles could be a promising delivery system for the therapy of metastatic breast cancer.

Keywords: metastasis, dual-targeting, breast cancer therapy, reduction-sensitive micelles, drug delivery

Introduction

Breast cancer is the most common malignancy in women, seriously threatening their health and lives.[1] Especially, metastasis is responsible for more than 90% of cancer-related deaths, and it is a severe issue in cancer management.[2,3] Tumor metastasis is a comprehensive and multifactorial process with the invasion-metastasis cascade. Although significant progress has been made in early detection and treatment, the prognosis has not been completely improved in metastatic breast cancer patients.[4,5] Until now, satisfactory strategies have not been found. As a result, the inhibition of tumor metastasis is still a great challenge in anticancer therapy.

Chemotherapy is one of the conventional treatment methods for many cancers. It is the first choice to suppress invasive breast cancer. Due to the non-selectivity and side effects of chemotherapeutic drugs, their applications were widely limited in clinics. To solve this issue, polymeric micelles have received increasing attention as drug carriers in

Received: 30 November 2022
Accepted: 27 January 2023
Published: 10 February 2023

© 2023 Yu et al. This work is published and licensed by Dove Medical Press Limited. The full terms of this license are available at https://www.dovepress.com/terms.php and incorporate the Creative Commons Attribution – Non Commercial (unported, v3.0) License (http://creativecommons.org/licenses/by-nc/3.0/). By accessing the work you hereby accept the Terms. Non-commercial uses of the work are permitted without any further permission from Dove Medical Press Limited, provided the work is properly attributed. For permission for commercial use of this work, please see paragraphs 4.2 and 5 of our Terms (https://www.dovepress.com/terms.php).

Graphical Abstract

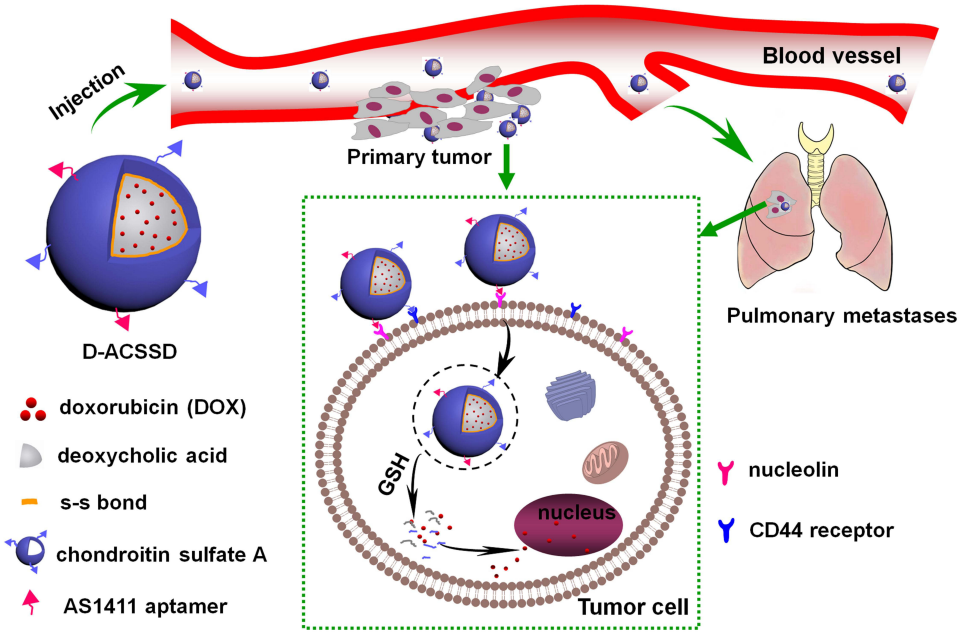

anticancer therapy.[6,7] Amphiphilic copolymers have the characteristics of low toxicity, biocompatibility, high flexibility, etc. The nano-sized micelles can reduce side effects and increase treatment efficiency through the enhanced permeation and retention (EPR) effect.[8,9]

Recently, smart delivery nanosystems with the properties of targeted and controlled drug release have been designed.[10,11] For example, reduction-responsive micelles could trigger rapid drug release under intracellular tumor compartments.[12] Reduced glutathione (GSH) levels in the tumor cells showed greatly higher than that in normal cells. Under the reduced environment, it provides the rapid breakage of the disulfide bonds within the polymeric nanoparticles.[13–15] Therefore, reduction-sensitive drug delivery systems have attracted extensive attention in cancer therapy. As previously reported by our group, chondroitin sulfate A conjugated deoxycholic acid (CSSD) micelles with disulfide linkages exhibited rapid release of antitumor drug in tumor intracellular environment with high concentrations of GSH.[16] Chondroitin sulfate A (CSA) is a kind of natural and biodegradable materials, and its derivatives have been investigated and used as active targeting vehicles in CD44 receptor-overexpressed tumor cells.[17–19] Deoxycholic acid (DOCA) is a bile acid that can emulsify and solubilize dietary fats in our bodies. Then, both CSA and DOCA exhibit good biocompatibility. In order to further improve the drug efficacy in vitro and in vivo, dual-targeting nano-systems could be designed and developed.[20,21]

Aptamers are single-stranded RNA or DNA ligands and have been employed as an active targeting group on the surface of some nanosystems.[22] AS1411 is a DNA aptamer that has a specific affinity and selectivity to nucleolin. Nucleolin is a kind of phosphoprotein in the cytoplasm and nucleus, particularly overexpressed on the membrane of tumor cells.[23,24] AS1411-modified nanoparticles could facilitate drug transport and cellular internalization by tumor cells via specific recognition of nucleolin.[25–27] These nanoparticles have been widely used in cancer therapy, such as lung cancer, prostate cancer, and metastatic renal cell carcinoma. However, there were fewer reports about AS1411-modified micelles for the inhibition of breast cancer metastasis.

In this work, the objective is to construct dual-targeting and reduction-sensitive polymeric micelles for improved drug delivery against breast cancer growth and metastasis. Novel AS1411 aptamer-modified CSSD (ACSSD) conjugate was synthesized. Doxorubicin (DOX) was encapsulated into ACSSD micelles, and the obtained D-ACSSD micelles were

evaluated. The therapeutic efficacy of D-ACSSD micelles was investigated in metastatic breast carcinoma. The in vitro efficacy and the effect on the cell functions, including cell proliferation, cell invasion and migration were studied. Furthermore, the inhibition activities of tumor growth and metastasis were performed in 4T1-bearing orthotopic mice.

Methods

Synthesis of AS1411 Aptamer-Modified Conjugate

The synthetic routes of AS1411-containing ACSSD are shown in Figure 1. Briefly, CSSD was synthesized by our previous report with some modifications.[16] DOCA (2.0 g) and EDC (2.93 g) were placed into a flask and dissolved in 80 mL ethanol. Cystamine dihydrochloride (2.3 g) in distilled water was slowly dropped into the above solution. After 24 h stirring, the reacted solution was concentrated on a rotary evaporator in vacuo. The resulting solution was deposited at −20 °C and rinsed with ice-cold water. Then, DOCA conjugated cystamine (DOCA-Cys) was produced by drying under vacuum conditions. Next, 1.0 g CSA was dissolved in 20 mL of distilled water. EDC (0.165 g) and DOCA-Cys (0.19 g) in 20 mL ethanol were slowly introduced into the CSA solution. After 24 h reaction, the mixture was transferred into dialysis bags for dialysis as stated above. Further, the solution was freeze-dried for 72 h and CSSD was obtained. In the third step, for AS1411 conjugation, the carboxyl units of CSSD were activated. CSSD (50 mg) was dispersed in 5 mL distilled water and 8 mL dimethyl sulfoxide (DMSO). EDC (10.9 mg) was added. AS1411 (30 OD, oligonucleotide sequence: 5′-NH_2-GGTGGTGGTGGTTGTGGTGGTGGTGG-3′) was dissolved in the mixture of DMSO and distilled

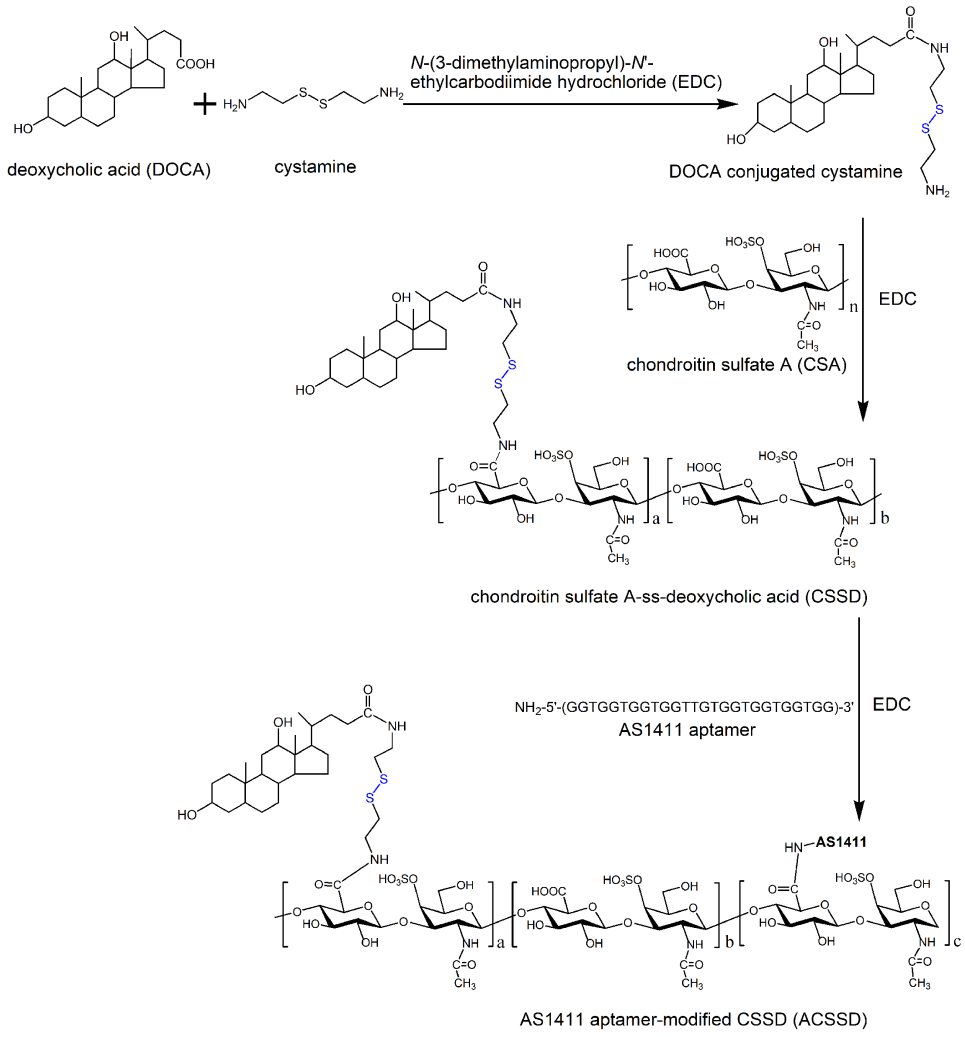

Figure 1 Synthetic scheme of ACSSD conjugate.

water and introduced into the above solution under stirring. After 24 h, the reaction solution was dialyzed against water and lyophilized.

The chemical structures of copolymers were analyzed by FTIR spectroscopy (Bruker Tensor II, Germany) and ^{1}H NMR spectroscopy (Bruker DMX 500 spectrometer, Germany). The conjugation ratio of DOCA groups in the conjugate was studied by an elemental analyzer (Vario Micro Cube, Elementar, Germany). The critical micelle concentration (CMC) value of the copolymer was analyzed by using a pyrene fluorescence probe. The fluorescent spectra were measured by a Hitachi F-7000 spectrophotometer.

Preparation of Drug-Containing Micelles

The dialysis method was employed for the preparation of DOX-encapsulated micelles. Typically, 50 mg of CSSD or ACSSD were dispersed in 20 mL of deionized water and DMSO (1:1, v:v). DOX·HCl (10 mg) was neutralized by 7.2 μL triethylamine in DMSO overnight and introduced into the copolymer suspensions under stirring. After 6 h, the mixed solution was transferred to a dialysis bag (MWCO: 14 kDa) and dialyzed for 24 h. Finally, the dialysis solution was filtered and freeze-dried.

Characterization of Drug-Free or Drug-Containing Micelles

The particle size and zeta potentials of blank or DOX-containing micelles were detected by a zeta sizer (90Plus, Brookhaven Instruments Corp., USA). Blank or DOX-containing micelles were dispersed in aqueous media at 25 °C. The concentration of the nanoparticles was set at 1.0 mg/mL. Particle size analysis was done at a scattering angle of 90 ° C. The shape images were detected by using transmission electron microscopy (TEM, JEM-2010, Jeol, Japan) at 80 kV. The amount of DOX in the micelles was analyzed by ultraviolet spectrophotometer. The absorbance was detected at 480 nm. Subsequently, the DOX-loading content (LC) and encapsulation efficiency (EE) were determined by using the following equations:

$$\mathrm{LC} = \frac{\text{amount of DOX in the micelles}}{\text{amount of DOX} - \text{containing micelles}} \times 100\% \quad (1)$$

$$\mathrm{EE} = \frac{\text{amount of DOX in the micelles}}{\text{amount of feed DOX}} \times 100\% \quad (2)$$

In vitro release behavior of DOX was studied in phosphate-buffered saline (PBS, pH 7.4) with or without 10 mM GSH at 37 °C. Briefly, 1 mL of free DOX or DOX-containing micelles was sealed in a dialysis bag and immersed with 20 mL of fresh release media in a plastic tube. The condition was maintained in an air-bath shaker at a speed of 150 rpm. At selected time intervals, the dialysis media were removed and replenished with 20 mL of fresh media. The DOX concentration in the media was investigated by a fluorescence spectrophotometer. The excitation and emission wave-numbers were made at 470 and 585 nm, respectively.

Cell Culture

Murine 4T1 cells were provided by China Center for Type Culture Collection (Wuhan, China). MDA-MB-231 cells were obtained from National Collection of Authenticated Cell Cultures (Shanghai, China). These cells were cultured in RPMI-1640 media with 10% FBS and 1% penicillin-streptomycin. The culture conditions were in a humidified atmosphere with 5% CO_2.

In vitro Cellular Uptake

4T1 cells were seeded at 3.0×10^4 cells per well in 24-well plates and grown for 48 h. After the culture media were removed, the cells were incubated in RPMI-1640 media with D-CSSD, D-ACSSD micelles or DOX·HCl. The final DOX concentration was 5.0 μg/mL. After 4 h incubation, the drug-containing media were discarded. The cells were washed with PBS (pH 7.4), and Hoechst 33,342 (10 μg/mL) was added. After staining for 0.5 h, the cells were fixed with 4% paraformaldehyde. Thereafter, 4T1 cells were rinsed with PBS, and the images were captured by confocal laser scanning microscope (CLSM, Leica SP8, Germany).

In vitro Cytotoxicity

4T1 or MDA-MB-231 cells were seeded at a density of 5000 cells/well in 96-well plates. After the cells adhered to the bottom of the plates, the original media were replaced with fresh media containing DOX·HCl, drug-free or DOX-containing polymeric micelles. After 24 or 48 h incubation, the media in each well were discarded. 100 μL of MTT solution was added and incubated with the cells for 4 h. Subsequently, the media were removed and 150 μL DMSO was added. The purple crystals were dissolved for 15 min at 37 °C. The absorbance was recorded at 490 nm by using a microplate reader.

In vitro Inhibition Activity on Cell Migration and Invasion

The wound-healing assay was adopted to investigate the ability of cell migration.[28] In brief, 4T1 cells were seeded in 12-well plates and grown until reaching nearly 85% confluence. Plastic pipette tips were used to generate scratch wounds in the cell monolayer. 4T1 cells were washed with cold PBS and followed by incubation with fresh medium (as a control), DOX·HCl, D-CSSD or D-ACSSD micelles. The equivalent concentration of DOX was 1.0 mg/mL. After incubation, the cells were recorded and counted by a microscope.

The invasion assay was performed in 4T1 cells in an insert Transwell device.[29] In brief, the upper chambers were pre-coated with diluted Corning Matrigel® (1:5, 0.1 mL/well) by serum-free media. 4T1 cells (1.0×10^6) in 0.1 mL of serum-free media were added. The lower chambers were supplemented with 0.6 mL of culture media with 10% FBS. DOX·HCl, D-CSSD or D-ACSSD micelles (equivalent DOX concentration: 1.0 mg/mL) were introduced into both chambers. After 24 h incubation, the migrated cells on the lower surface of the Transwell chambers were fixed with methanol. For staining, 0.1% crystal violet was added. The cells were observed and counted by using light microscopy.

In vivo Antitumor Effects

Female BALB/c mice were provided by Hunan SJA Laboratory Animal Co., Ltd (Changsha, China). The age was 4–6 weeks. The animal experiments were approved by the Experimental Ethics Committee of Jiujiang University (Approval No. 2021-YX-027). All animal studies were made by the guidelines for the Ethical Review of Laboratory Animal Welfare in China (GB/T35892-2018). The breeding conditions of laboratory animals were performed according to the requirements of the environment and housing facilities in China (GB 14925–2010).

The orthotopic 4T1 cancer model was established in female BALB/c mice. In brief, 4T1 cells (1.0×10^7/mice) were subcutaneously injected into the mammary fat pad of mice. The tumor size was recorded by vernier caliper. The volume (V) was calculated by the following equation: $V = 0.5 \times a \times b^2$, where a and b were the length and width of the tumors, respectively. As the tumor size was up to ~1500 mm^3, mice were sacrificed. The tumors were taken out and cut into ~30 mm^3 parts. Then the small tumor was implanted subcutaneously at the mammary fat pad of healthy mice.[30] The drug administrations were initiated as the tumor volumes were nearly 150 mm^3. Orthotopic 4T1-bearing mice were randomly assigned to 6 groups (n = 5). 5% glucose, DOX·HCl, CSSD, ACSSD, D-CSSD and D-ACSSD were intravenously injected into mice every 5 days. The first day of drug injection was set as day 0. The equivalent DOX dose was 5.0 mg/kg. The injection amounts of drug-free micelles were 40 mg/kg, which was approximately equivalent to the amounts of copolymers in DOX-containing nanoparticles. The body weight and tumor size were determined every day.

At the end of the experiment, mice were sacrificed. The main organs were collected and fixed with 10% formaldehyde solution. Then, they were embedded in paraffin. After a series of treatments, hematoxylin and eosin (H&E) staining was made on the slices. Some of these sections were applied to investigate apoptosis by the TdT-mediated dUTP nick end labeling (TUNEL) method. The procedures were done according to the manufacturer's protocols (Beyotime Biotechnology, Shanghai, China).

Statistical Analysis

The numerical data were shown as mean ± SD for all groups. Statistical analysis was determined by a one-way ANOVA. $P < 0.05$ and $P < 0.01$ were defined as significant and very significant differences, respectively.

Results and Discussion

Synthesis and Characterization of AS1411 Aptamer-Modified Conjugate

As shown in Figure 1, ACSSD conjugate was synthesized by the amidation reactions between carboxyl moieties of the CSA backbone and primary amines of DOCA-Cys or AS1411 aptamer. EDC is generally used as a zero-length crosslinker to couple carboxyl groups to amino groups. First, DOCA was synthesized with cystamine dihydrochloride, and DOCA-Cys with a disulfide bond was obtained. Then, CSA was reacted with DOCA-Cys, leading to the formation of CSSD copolymer with reduced disulfide linkers. Further, ACSSD was synthesized by conjugating 5'-NH_2-AS1411 with CSSD. The chemical structures of CSSD and ACSSD were analyzed by FTIR and ^{1}H NMR. As shown in Figure 2A, a shoulder peak was observed at 1702 cm^{-1} (C=O stretching vibration) in CSSD copolymer. It inferred that CSSD was synthesized. Compared with CSSD, the new peak of ACSSD appeared at 926 cm^{-1} which was assigned to the C-H vibrations of AS1411 aptamer. These results evidenced that ACSSD had been synthesized. As presented in Figure 2B, CSSD was confirmed by the conjugated DOCA groups at 0.66–1.86 ppm and the disulfide bond linker at 2.88 ppm.[16] The peak intensity of ACSSD at 0.77 ppm increased as compared to CSSD. Additionally, a new peak of ACSSD copolymer appeared at 2.39 ppm. These results suggested that ACSSD was successfully synthesized. The grafted ratio of DOCA was determined by element analysis. In the CSSD copolymer, 100 sugar units of CSA were conjugated with 7.9 DOCA groups.

To investigate the ability of self-assembly, the CMC value of ACSSD was studied by fluorescence analysis of pyrene. As presented in Figure 2C, the CMC value of ACSSD copolymer was 0.076 mg/mL. Such low CMC value ensured that the copolymer can spontaneously form self-assembled micelles and be stable in highly diluted conditions. The TEM image demonstrated that the morphology of ACSSD micelles was almost spherical (Figure 2D). The particle size of blank ACSSD micelles was 355 nm determined by DLS (Table 1), which was larger than that analyzed by TEM. It is partly ascribed to the different processes of sample preparation. The TEM particles were in a dried state, whereas the nanoparticles analyzed by DLS were in a hydrated state. In addition, the particle diameter of CSSD was 364 nm (Table 1). It indicated that ACSSD was almost the same size as CSSD. The zeta potentials of CSSD and ACSSD were −41.8 and −40.5 mV, respectively. As stated, the negative potentials were beneficial for passive targeting by the EPR effect and prevention of rapid clearance of the micelles in vivo.[17]

Amphiphilic copolymer could form self-assembled aggregates in aqueous media. By using a dialysis method, the DOX base was encapsulated into the core of CSSD or ACSSD micelles. As shown in Table 1, the loading content of

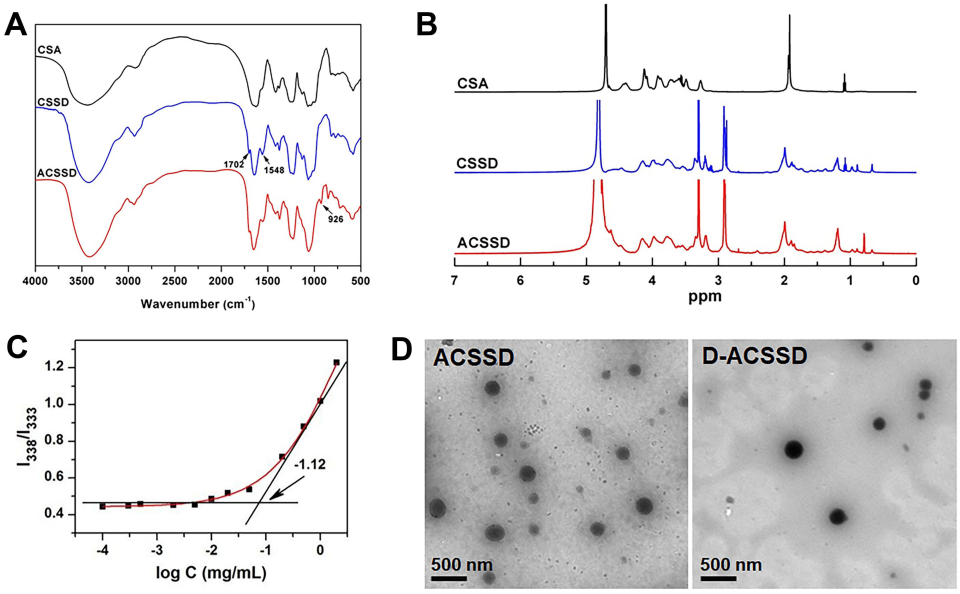

Figure 2 (**A**) FTIR patterns of CSA, CSSD and ACSSD. (**B**) ^{1}H NMR spectra of CSA, CSSD and ACSSD. (**C**) Plot of the I_{338}/I_{333} ratio vs log C from pyrene excitation spectra of ACSSD. (**D**) TEM photos of ACSSD and D-ACSSD.

Table 1 Physicochemical Characteristics of Drug-Free and Drug-Containing Micelles

Sample	Particle Size (nm)[a]	Polydispersity Index	Zeta Potentials (mv)	LC (%)	EE (%)
CSSD	364 ± 29.3	0.159 ± 0.02	−41.8 ± 1.2	–	–
ACSSD	355 ± 26.1	0.152 ± 0.02	−40.5 ± 1.7	–	–
D-CSSD	311 ± 22.7	0.156 ± 0.02	−42.3 ± 2.4	14.2 ± 1.0	85.4 ± 6.1
D-ACSSD	295 ± 29.4	0.188 ± 0.03	−40.1 ± 2.3	13.7 ± 1.3	82.2 ± 7.9

Note: [a]Measured by DLS.

D-CSSD and D-ACSSD micelles were 14.2% and 13.7%, respectively. The encapsulation efficiency of DOX in the micelles was >80%, which indicated that the drug was well incorporated. The diameters of D-CSSD and D-ACSSD determined by DLS were 311 and 295 nm, respectively. The sizes of drug-containing micelles were smaller than those of their counterpart drug-free micelles. The micelles after drug loading become compact. This shrinkage phenomenon is attributed to the improved interaction between hydrophobic groups of the conjugates and DOX base. A similar result was stated by other researchers.[31] The zeta potentials of D-CSSD and D-ACSSD micelles were −42.3 and −40.1 mV, respectively. TEM image displayed the spherical-shaped structure of D-ACSSD micelles (Figure 2D). These nanoparticles were expected to have a good ability to accumulate at tumor sites.

In vitro Drug Release

The release behaviors of DOX from drug-containing micelles were investigated in PBS (pH 7.4) in the presence or absence of 10 mM GSH, simulating the body fluid. The results are presented in Figure 3. Free DOX was completely released within 8 h in PBS (pH 7.4). It revealed that free drugs diffused from a dialysis bag into the media speedily. Meanwhile, DOX release from D-CSSD and D-ACSSD micelles were 54.4% and 52.3% in 96 h, respectively. There were no pronounced differences in these drug-encapsulating micelles. It inferred that AS1411 aptamer modification did not affect drug release. This incomplete drug-releasing behavior of DOX-loaded micelles might be attributed to the hydrophobic interactions between DOX molecules and the hydrophobic segments.[32,33] In addition, the cumulative DOX

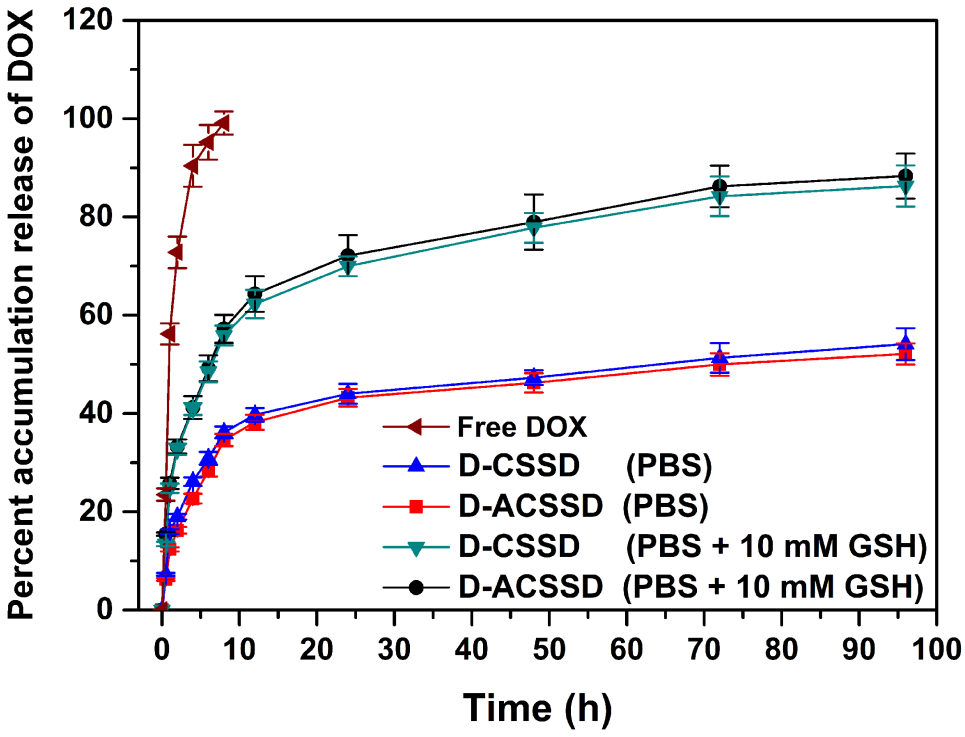

Figure 3 Release curves of DOX from free DOX, D-CSSD or D-ACSSD micelles in PBS (pH 7.4) or PBS (pH 7.4, 10 mM GSH) at 37 °C.

release rate from D-CSSD was 86.7% for 96 h in PBS containing 10 mM GSH, which was more ($P < 0.05$) than that in PBS without GSH. Under the same conditions containing GSH, approximately 88.3% of DOX was released from D-ACSSD. These results indicated that reduced GSH was attributed to the breakage of the disulfide bond linker in the copolymers, leading to a quick drug release. We inferred that the D-CSSD and D-ACSSD micelles had reduction-responsive characteristics and could increase drug concentrations in the tumor cells.

In vitro Cellular Uptake

Given that cell entry efficiency and intracellular release are very important for the therapeutic activities of antitumor drugs, we further studied the cellular uptake of DOX-containing micelles. Three DOX-based formulations were incubated with 4T1 cells for 4 h. By CLSM observations (Figure 4), DOX emitted red fluorescence, and Hoechst 33,342 showed blue fluorescence in the nucleus. DOX·HCl exhibited the strongest red fluorescence among these DOX formulations. Similar results were described by some researchers.[34,35] DOX-containing micelles with red fluorescence were mostly distributed in the cytoplasm, whereas DOX·HCl was seen mainly in the nucleus. These results were mostly due to that free DOX·HCl could quickly diffuse into the cells, and drug-containing polymeric micelles were entered into 4T1 cells in an endocytosis manner. It appeared different amounts of DOX accumulation in the intracellular cells. As described above, DOX-containing polymeric nanoparticles have large particle sizes and high molecular weight. It leads to low DOX accumulation and a slow rate of drug release in 4T1 cells. Further, these results were in accord with the above drug release in vitro. Importantly, D-ACSSD micelles demonstrated stronger red spots in 4T1 cell lines, revealing a higher uptake than D-CSSD micelles. The improved cellular uptake of D-ACSSD was largely due to the targeting interactions between the AS1411 aptamer and the nucleolin of 4T1 cells.[36]

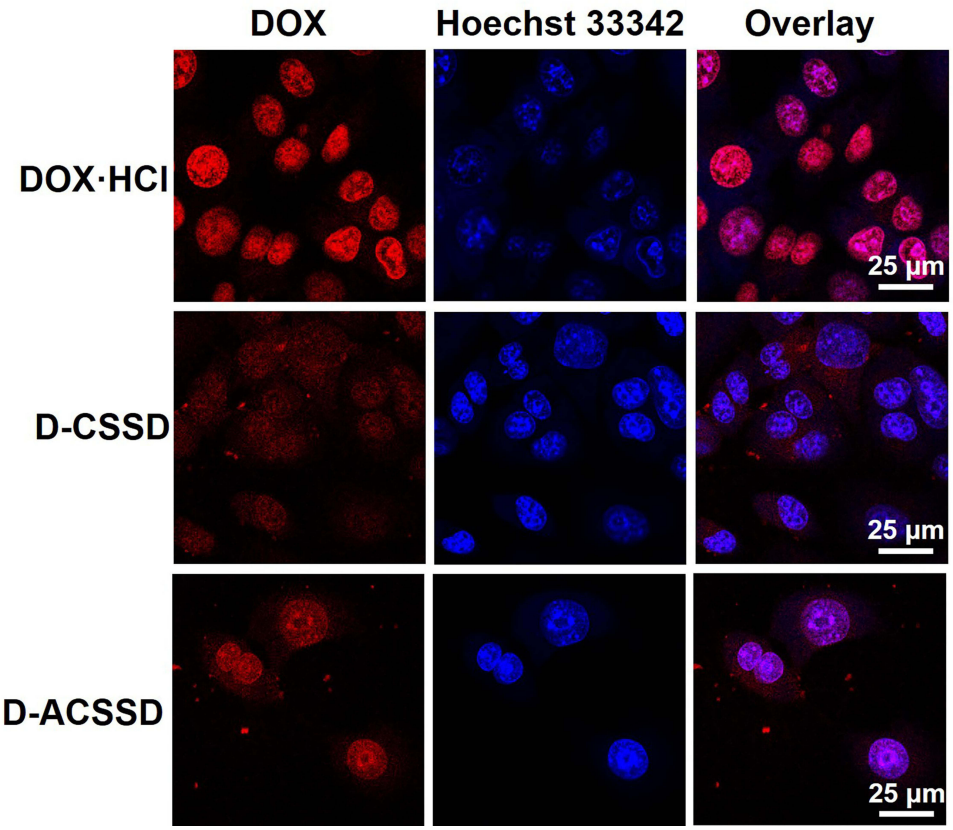

Figure 4 CLSM images of DOX·HCl, D-CSSD and D-ACSSD micelles incubated in 4T1 cells for 4 h.

In vitro Cytotoxicity

In vitro antitumor activities of drug-containing micelles were comparatively studied against 4T1 and MDA-MB-231 cells by the MTT method. It is known that both MDA-MB-231 and 4T1 cells are CD44-receptor positive and highly metastatic.[37,38] As presented in Figure 5, DOX-based formulations exhibited dose-dependent killing activities. The half-inhibitory concentration (IC_{50}) values of D-CSSD, D-ACSSD and DOX·HCl were 4.98, 3.82 and 0.91 μg/mL against MDA-MB-231 cells at 24 h, respectively (Table 2). Additionally, the IC_{50} value of DOX·HCl was 1.62 μg/mL in 4T1 cells for 24 h treatment, which was 2.75 and 1.94-times lower than that obtained for D-CSSD and D-ACSSD micelles, respectively. It is known that DOX molecules are attributed to the toxic effect. The results exhibited that DOX·HCl exerted the strongest cytotoxic effect against 4T1 and MDA-MB-231 cells in vitro. Similar phenomena were described by other researchers.[39,40] It was partly ascribed to the quick diffusion of free DOX·HCl and the slow drug release of DOX-containing micelles. It agreed with the results of CLSM observations. Notably, the IC_{50} of D-ACSSD was lower ($P<0.05$) than that of D-CSSD micelles in MDA-MB-231 and 4T1 cells. This was attributed to the improved cellular uptake and targeted nucleolin of D-ACSSD in these cells.

The antitumor tendencies of DOX-containing nanoparticles were further evaluated at the time point of 48 h. As shown in Figures 6A and 6B, the inhibition activities of three DOX formulations were time- and concentration-dependent. In MDA-MB-231 cells, the IC_{50} values of DOX·HCl, D-CSSD or D-ACSSD were 0.27, 0.95 or 0.41 μg/mL at 48 h, respectively (Table 2). D-ACSSD was significantly stronger inhibition than D-CSSD ($P < 0.01$). In addition, the IC_{50} value of D-ACSSD was 1.50-fold lower than that of D-CSSD ($P < 0.05$) in 4T1 cells at 48 h (Table 2). These results were ascribed to selectively targeting nucleolin of D-ACSSD as described above. In addition, blank CSSD and ACSSD did not show cytotoxicity against MDA-MB-231 and 4T1 cells at the equivalent polymer concentration of D-CSSD and D-ACSSD (Figures 5 and 6). These results suggested that D-ACSSD could effectively deliver DOX into the tumor sites in a nucleolin and CD44 receptor-targeting manner.

In vitro Inhibition Activity on Cell Migration and Invasion

Cancer metastasis is a complex and multi-step process. It comprises the detachment of cancer cells from the primary tumor site, migration and invasion at the initial stage.[41] As previously reported, AS1411 was evaluated for the treatment of metastatic renal cell carcinoma.[42] Herein, a wound-healing assay was employed to investigate the inhibition capability of D-ACSSD micelles on the migration of 4T1 cells. The wound closure was recorded at 0 and 24 h. As shown in

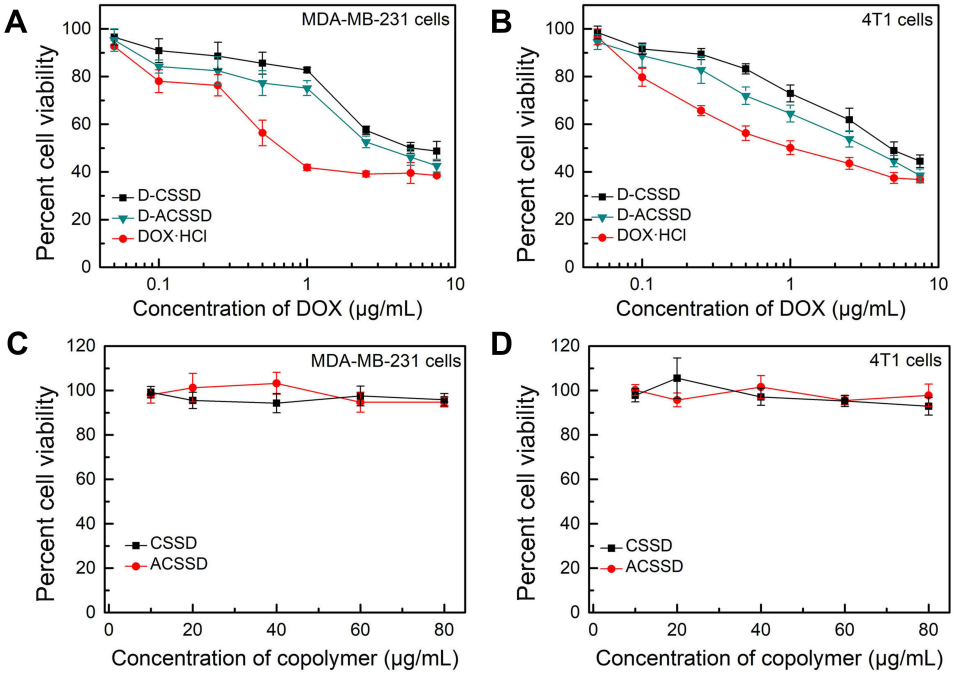

Figure 5 In vitro cytotoxicity of D-CSSD, D-ACSSD, DOX·HCl, blank CSSD and ACSSD micelles in (**A** and **C**) MDA-MB-231 and (**B** and **D**) 4T1 cells for 24 h.

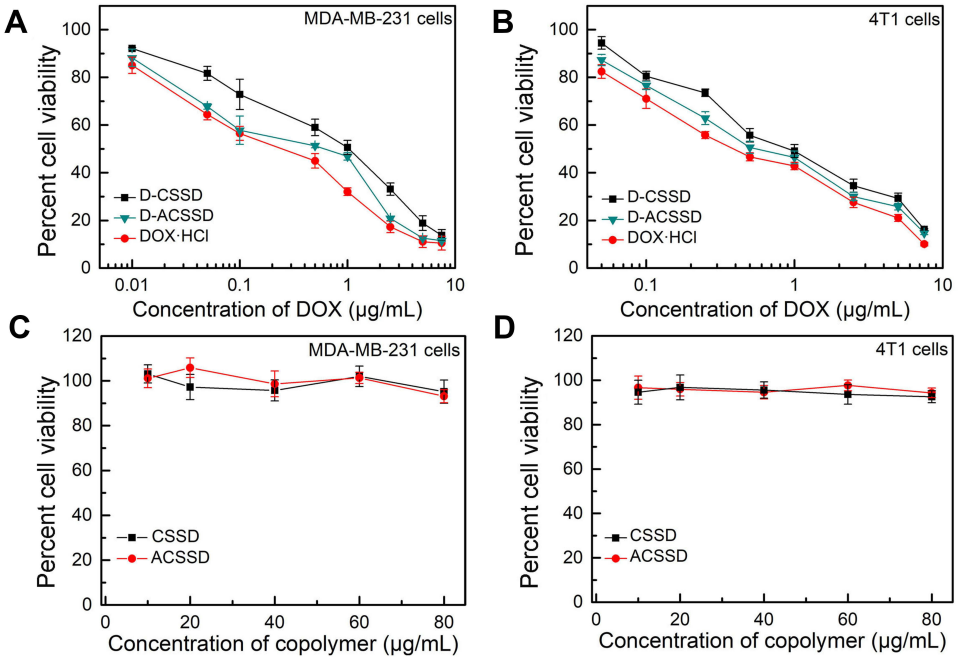

Figure 6 In vitro cytotoxicity of D-CSSD, D-ACSSD, DOX·HCl, blank CSSD and ACSSD micelles in (**A** and **C**) MDA-MB-231 and (**B** and **D**) 4T1 cells for 48 h.

Figure 7, the average healing rate of cultured media reached 74.3% and was reduced by DOX formulations. The wound-healing rates of DOX·HCl, D-CSSD and D-ACSSD micelles were reduced to 27.0%, 63.5% and 44.5%, respectively. In addition, the healing rate of D-ACSSD was lower than that of D-CSSD ($P < 0.05$). It was due to the AS1411 targetability of D-ACSSD in 4T1 cells. It agreed with the results of cytotoxicity in vitro.

The cell invasion assay was conducted by using Transwell chambers with pre-coating matrigel, simulating to allow the tumor cells to degrade the extracellular matrix barrier and migrate through the vessels.[43] As shown in Figure 8, 4T1 cells in the cultured media group easily invaded the lower chamber. DOX·HCl, D-CSSD and D-ACSSD micelles inhibited cell invasion to varying degrees, which were 24.5%, 41.1% and 77.2%, respectively. Especially, D-ACSSD micelles exhibited better inhibitory effects on the metastasis of 4T1 cells than D-CSSD micelles ($P<0.05$). The effect of D-ACSSD micelles might be attributed to the active targeting activity by AS1411 aptamer and improved intracellular DOX concentration.[24] Therefore, D-ACSSD micelles could effectively enhance the inhibition of migration and invasion of 4T1 cells after AS1411 modification.

In vivo Antitumor Effects

The 4T1 orthotopic mice model was established by implanting cancer cells into the breast pad of mice. Then, the original tumor was dissected and cut into small parts. Further, the small tumors were inoculated into the breast pad of mice. In vivo antitumor activities were carried out on 4T1 orthotopic mice with lung metastases. The mice received an intravenous injection of 5% glucose, blank micelles, DOX·HCl, D-CSSD or D-ACSSD micelles. The primary tumor

Table 2 IC_{50} Values of DOX·HCl, D-CSSD and D-ACSSD in MDA-MB-231and 4T1 Cells (n = 3)

Sample (μg/mL)	MDA-MB-231		4T1	
	24 h	48 h	24 h	48 h
DOX·HCl	0.91±0.14	0.27±0.04	1.62±0.29	0.46±0.05
D-CSSD	4.98±0.59	0.95±0.13	4.45±0.63	1.02±0.14
D-ACSSD	3.82±0.42	0.41±0.06	3.14±0.45	0.68±0.07

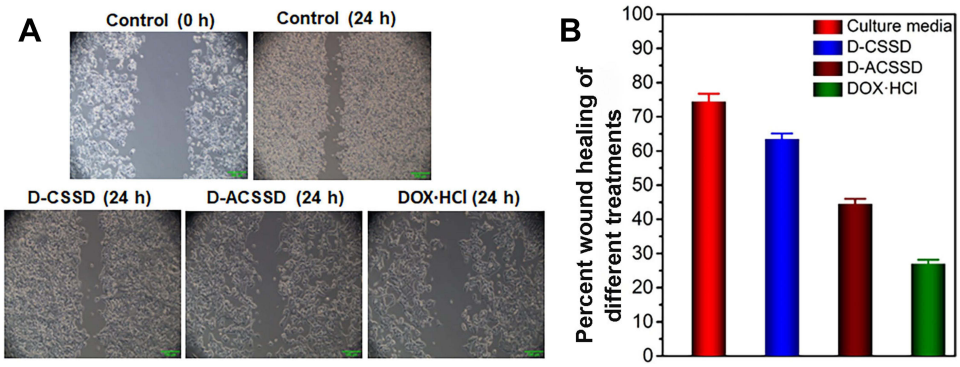

Figure 7 (**A**) Typical images and (**B**) quantified wound healing inhibitory effect of culture media (control), D-CSSD, D-ACSSD and DOX·HCl in 4T1 cells.

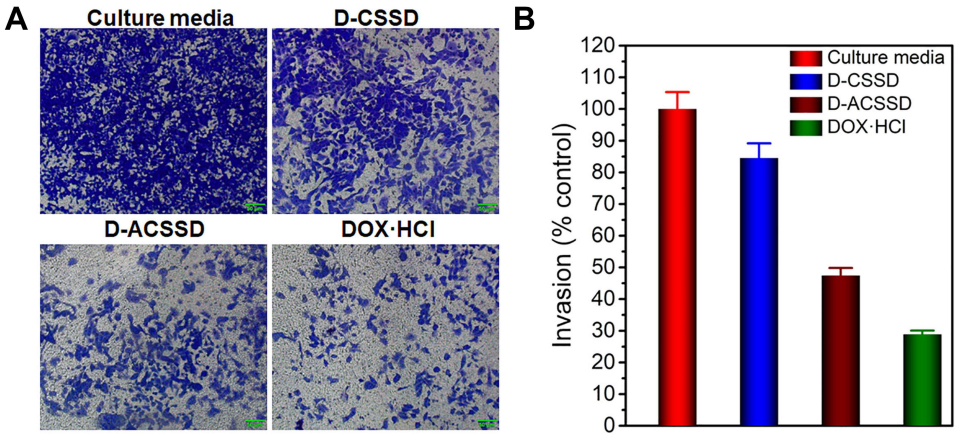

Figure 8 (**A**) Typical images and (**B**) quantified invasion effect of culture media, D-CSSD, D-ACSSD and DOX·HCl in 4T1 cells.

size and body weight were measured during the whole treatment period. The change rate of tumor volume in the mammary was based on the start point (Figure 9). As expected, the tumor volumes in the groups of 5% glucose, CSSD and ACSSD greatly increased throughout the experiment (Figure 9A). The differences among these groups were not significant ($P > 0.05$). However, three DOX-containing groups exhibited extremely significant differences in the inhibition of tumor growth compared with 5% glucose group ($P < 0.001$). More importantly, D-ACSSD micelles showed the strongest effect on tumor inhibition in contrast with D-CSSD micelles ($P < 0.05$) and DOX·HCl ($P < 0.01$). As previously reported, free drugs would be rapidly cleared from blood circulation in vivo, leading to a short half-life time and low area under the curve.[44] Drug-encapsulated micelles could prolong the circulation time in vivo, delay the clearance and concentrate the drug in targeted sites by the EPR effect.[29,45] Interestingly, the reduction-sensitive DOX release from D-CSSD or D-ACSSD micelles could increase the concentration of drug molecules in the intracellular cells. D-ACSSD micelles also could transport into the 4T1 tumor sites in dual nucleolin and CD44-targeting ways, demonstrating stronger pharmacological action than single-targeting D-CSSD micelles. As presented in Figure 9B, no obvious changes were detected in the body weights from all groups, and no statistical differences were detected.

The HE staining analysis was further to confirm the antitumor results. As shown in Figure 9C, the D-ACSSD group exhibited the maximum areas of cell necrosis and apoptosis. DOX·HCl and D-CSSD micelles induced mild tumor apoptosis. Furthermore, we assessed tumor cell apoptosis by TUNEL staining (Figure 9D). 5% glucose and blank micelle groups showed almost no green fluorescence in the primary tumors. Importantly, DOX-containing formulations emitted green fluorescence on different levels, indicating that nuclear DNA fragments produced during cell apoptosis. In particular, D-ACSSD micelles induced the highest rates of apoptosis, which was higher

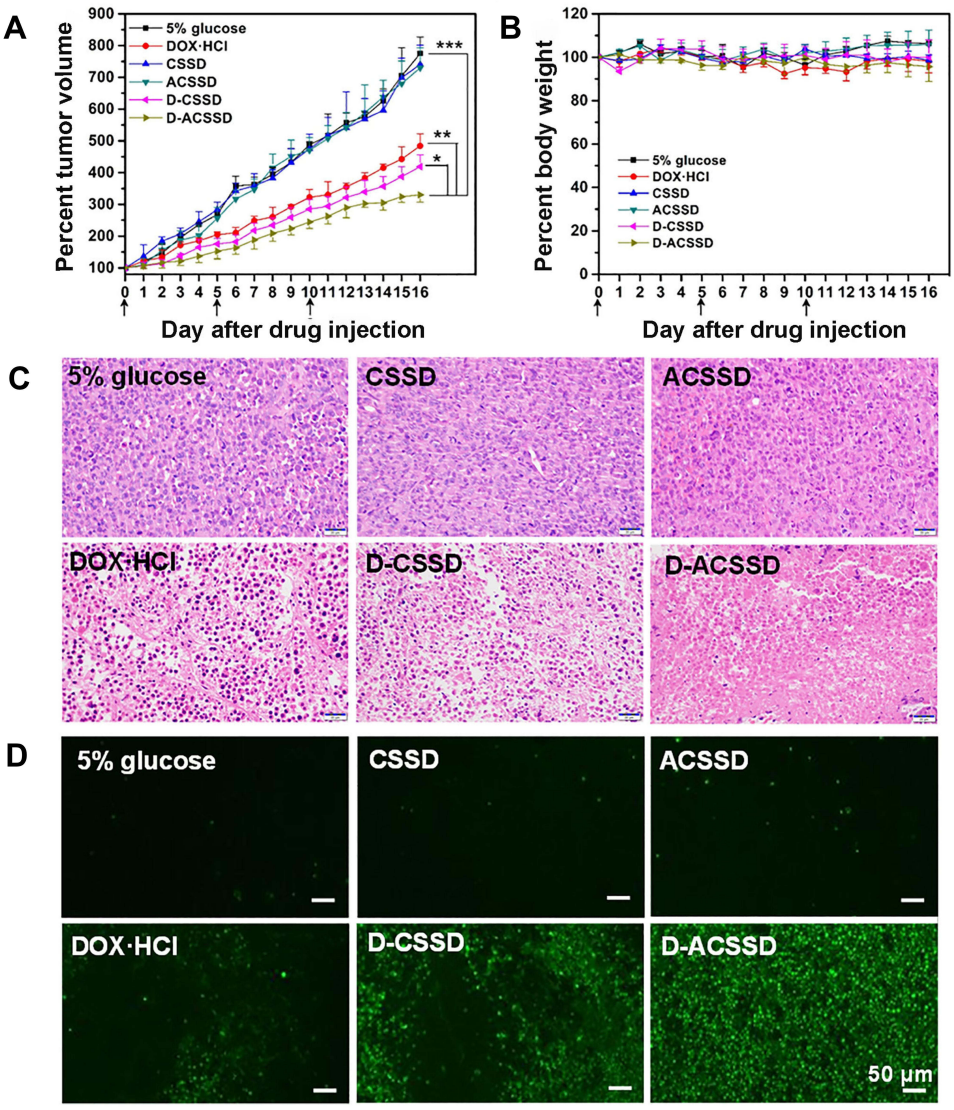

Figure 9 (**A**) Tumor growth curves and (**B**) body weight of orthotopic 4T1-bearing mice after the treatment with 5% glucose, DOX·HCl, CSSD, ACSSD, D-CSSD and D-ACSSD micelles (n = 5). (**C**) H&E and (**D**) TUNEL staining images of the tumors. *P < 0.05, **P < 0.01, ***P < 0.001.

than D-CSSD micelles and free DOX·HCl. The TUNEL results were consistent with those of tumor growth monitoring and HE staining. Therefore, the histological analysis provided more evidence for the outstanding therapeutic efficacy of dual targeting and reduction-sensitive D-ACSSD micelles.

As shown in Figure 10A, tumor metastatic nodules could be clearly observed on the surface of the lungs in 5% glucose, CSSD and ACSSD groups. Interestingly, the occurrence of lung metastasis in DOX-loaded micelles exhibited fewer metastases than that in DOX·HCl group. Surprisingly, no tumor nodules appeared in the lungs of D-ACSSD groups. These results indicated that AS1411-modified micelles had significant targeting effects and suppressed the lung metastasis of 4T1 tumors.[36] The pathological sections of lung tissues were seen to further study the inhibition of lung metastasis. As shown in Figure 10B, cancer nests were seen in the lung sections in 5% glucose and blank micelle groups but rarely observed in the D-ACSSD group. These results demonstrated that D-ACSSD micelles could simultaneously inhibit lung metastasis and primary tumor growth. Therefore, D-ACSSD could be an excellent drug system in the therapy of metastatic breast cancer.

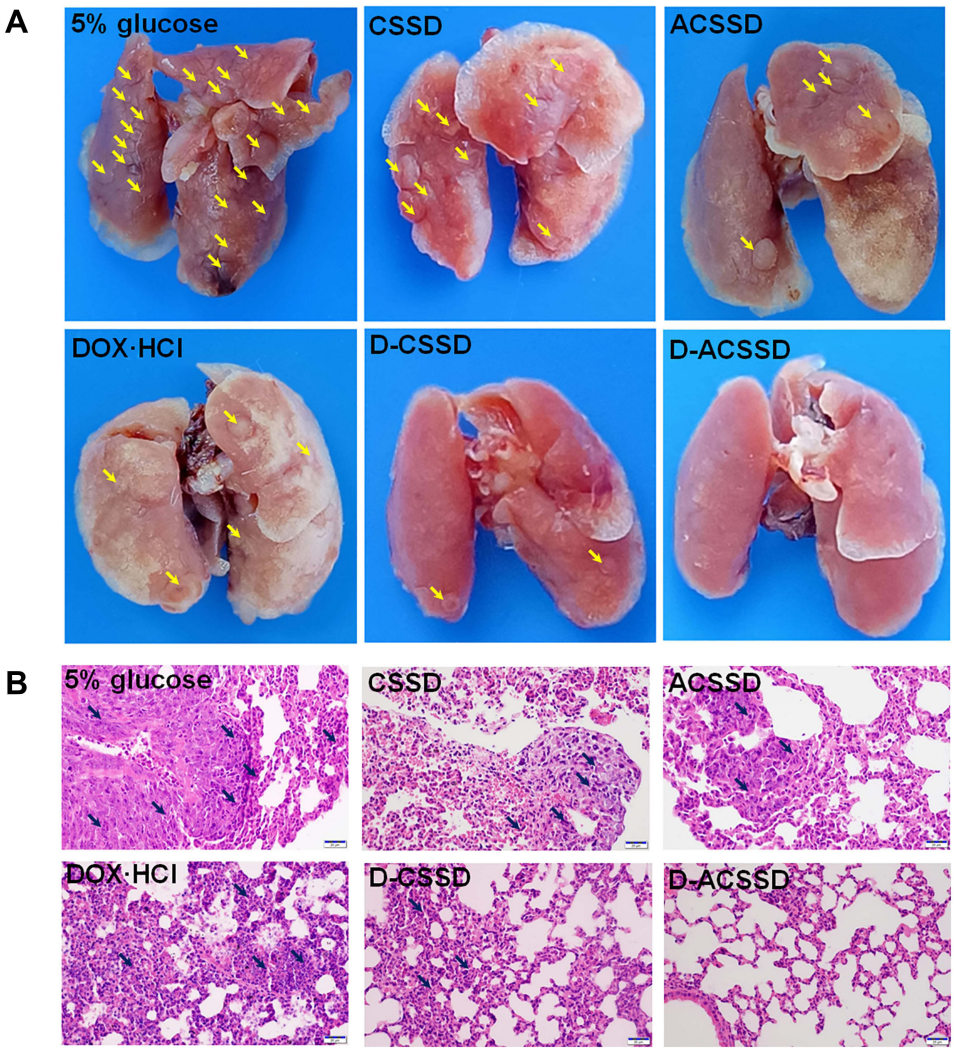

Figure 10 (**A**) Representative pictures of the lungs, and (**B**) H&E staining images of the lungs after administration of 5% glucose, DOX·HCl, CSSD, ACSSD, D-CSSD and D-ACSSD micelles in orthotopic 4T1-bearing mice. Yellow and black arrows represent lung metastases.

Conclusion

In summary, AS1411 aptamer-modified ACSSD micelles were successfully fabricated, and could effectively encapsulate DOX with good loading content. D-ACSSD micelles exhibited reduction-sensitive drug release in vitro and had higher inhibitory effects on the invasion and migration of 4T1 cells than D-CSSD. Notably, D-ACSSD micelles demonstrated stronger inhibition of antitumor activity and tumor metastasis in vivo, compared with free DOX·HCl and D-CSSD micelles. These results indicated that D-ACSSD would be an effective and smart delivery system against metastatic breast tumors. However, we did not explore the in-depth mechanism of D-ACSSD micelles in the tumor microenvironment in vivo. This is the focus of our future work.

Acknowledgments

This research was sponsored by the Natural Science Foundation of Jiangxi Province (20192ACBL20032 and 20202BABL206155), the Scientific Research Project of the Health Commission of Jiangxi Province (20204271and 202211975), and the Scientific Research Project of the Education Department of Jiangxi Province (GJJ180900 and GJJ201820).

Disclosure

The authors report no conflicts of interest in this work.

References

1. Siegel RL, Miller KD, Fuchs HE, Jemal A. Cancer statistics, 2022. *CA*. 2022;72:7–33. doi:10.3322/caac.21708
2. Jyotsana N, Zhang Z, Himmel LE, Yu F, King MR. Minimal dosing of leukocyte targeting TRAIL decreases triple-negative breast cancer metastasis following tumor resection. *Sci Adv*. 2019;5:eaaw4197. doi:10.1126/sciadv.aaw4197
3. Wang T-W, Yeh C-W, Kuan C-H, et al. Tailored design of multifunctional and programmable pH-responsive self-assembling polypeptides as drug delivery nanocarrier for cancer therapy. *Acta Biomater*. 2017;58:54–66. doi:10.1016/j.actbio.2017.06.008
4. Yu J, Mu Q, Fung M, Xu X, Zhu L, Ho RJY. Challenges and opportunities in metastatic breast cancer treatments: nano-drug combinations delivered preferentially to metastatic cells may enhance therapeutic response. *Pharmacol Ther*. 2022;236:108108.
5. Tang S, Meng Q, Sun H, et al. Dual pH-sensitive micelles with charge-switch for controlling cellular uptake and drug release to treat metastatic breast cancer. *Biomaterials*. 2017;114:44–53.
6. Jabbari A, Yaghoobi E, Azizollahi H, et al. Design and synthesis of a star-like polymeric micelle modified with AS1411 aptamer for targeted delivery of camptothecin for cancer therapy. *Int J Pharm*. 2022;611:121346.
7. Liu Y, Yu F, Dai S, et al. All-trans retinoic acid and doxorubicin delivery by folic acid modified polymeric micelles for the modulation of Pin1-mediated DOX-induced breast cancer stemness and metastasis. *Mol Pharm*. 2021;18:3966–3978.
8. Kaur J, Mishra V, Singh SK, et al. Harnessing amphiphilic polymeric micelles for diagnostic and therapeutic applications: breakthroughs and bottlenecks. *J Control Release*. 2021;334:64–95.
9. Ghosh B, Biswas S. Polymeric micelles in cancer therapy: state of the art. *J Control Release*. 2021;332:127–147.
10. Banstola A, Poudel K, Kim JO, Jeong J-H, Yook S. Recent progress in stimuli-responsive nanosystems for inducing immunogenic cell death. *J Control Release*. 2021;337:505–520. doi:10.1016/j.jconrel.2021.07.038
11. Chen WH, Yu X, Cecconello A, Sohn YS, Nechushtai R, Willner I. Stimuli-responsive nucleic acid-functionalized metal-organic framework nanoparticles using pH- and metal-ion-dependent DNAzymes as locks. *Chem Sci*. 2017;8:5769–5780. doi:10.1039/C7SC01765K
12. Sikder A, Vambhurkar G, Amulya E, et al. Advancements in redox-sensitive micelles as nanotheranostics: a new horizon in cancer management. *J Control Release*. 2022;349:1009–1030. doi:10.1016/j.jconrel.2022.08.008
13. Liu N, Tan Y, Hu Y, et al. A54 peptide modified and redox-responsive glucolipid conjugate micelles for intracellular delivery of doxorubicin in hepatocarcinoma therapy. *ACS Appl Mater Interfaces*. 2016;8:33148–33156. doi:10.1021/acsami.6b09333
14. Song Q, Wang X, Wang Y, et al. Reduction responsive self-assembled nanoparticles based on disulfide-linked drug-drug conjugate with high drug loading and antitumor efficacy. *Mol Pharm*. 2016;13:190–201. doi:10.1021/acs.molpharmaceut.5b00631
15. Ma ZC, Wu JP, Sun MC, Li BY, Yu X. Disulfur-bridged polyethyleneglycol/DOX nanoparticles for the encapsulation of photosensitive drugs: a case of computational simulations on the redox-responsive chemo-photodynamic drug delivery system. *RSC Adv*. 2021;11:37988–37994. doi:10.1039/D1RA05645J
16. Liu HX, Wu SQ, Yu JM, et al. Reduction-sensitive micelles self-assembled from amphiphilic chondroitin sulfate A-deoxycholic acid conjugate for triggered release of doxorubicin. *Mater Sci Eng C Mater Biol Appl*. 2017;75:55–63. doi:10.1016/j.msec.2017.02.030
17. Cai S, Xie X, Yuan Q, et al. Preparation and evaluation of reduction-responsive micelles based on disulfide-linked chondroitin sulfate A-tocopherol succinate for controlled antitumour drug release. *J Pharm Pharmacol*. 2021;73:1405–1417. doi:10.1093/jpp/rgab096
18. Lee J-Y, Chung S-J, Cho H-J, Kim -D-D. Phenylboronic acid-decorated chondroitin sulfate A-based theranostic nanoparticles for enhanced tumor targeting and penetration. *Adv Funct Mater*. 2015;25:3705–3717. doi:10.1002/adfm.201500680
19. Yu JM, Liang L, Xie X, et al. Multifunctional nanoparticles codelivering doxorubicin and amorphous calcium carbonate preloaded with indocyanine green for enhanced chemo-photothermal cancer therapy. *Int J Nanomedicine*. 2023;18:323–337. doi:10.2147/IJN.S394896
20. Yu JM, Xie X, Xu XY, et al. Development of dual ligand-targeted polymeric micelles as drug carriers for cancer therapy in vitro and in vivo. *J Mater Chem B*. 2014;2:2114–2126. doi:10.1039/c3tb21539c
21. Zhang XB, Wang Y, Wei GQ, Zhao JY, Yang G, Zhou SB. Stepwise dual targeting and dual responsive polymer micelles for mitochondrion therapy. *J Control Release*. 2020;322:157–169. doi:10.1016/j.jconrel.2020.03.011
22. Li X, Yu Y, Ji Q, Qiu LY. Targeted delivery of anticancer drugs by aptamer AS1411 mediated Pluronic F127/cyclodextrin- linked polymer composite micelles. *Nanomed Nanotechnol Biol Med*. 2015;11:175–184. doi:10.1016/j.nano.2014.08.013
23. Li L, Hou J, Liu X, et al. Nucleolin-targeting liposomes guided by aptamer AS1411 for the delivery of siRNA for the treatment of malignant melanomas. *Biomaterials*. 2014;35:3840–3850. doi:10.1016/j.biomaterials.2014.01.019
24. Zhang J, Chen R, Fang X, Chen F, Wang Y, Chen M. Nucleolin targeting AS1411 aptamer modified pH-sensitive micelles for enhanced delivery and antitumor efficacy of paclitaxel. *Nano Res*. 2015;8:201–218. doi:10.1007/s12274-014-0619-4
25. Yang S, Ren Z, Chen M, et al. Nucleolin-targeting AS1411-aptamer-modified graft polymeric micelle with dual pH/redox sensitivity designed to enhance tumor therapy through the codelivery of doxorubicin/TLR4 siRNA and suppression of invasion. *Mol Pharm*. 2018;15:314–325. doi:10.1021/acs.molpharmaceut.7b01093
26. Carvalho J, Lopes-Nunes J, Vialet B, et al. Nanoaggregate-forming lipid-conjugated AS1411 aptamer as a promising tumor-targeted delivery system of anticancer agents in vitro. *Nanomed Nanotechnol Biol Med*. 2021;36:102429. doi:10.1016/j.nano.2021.102429
27. Zhang F, Correia A, Makila E, et al. Receptor-mediated surface charge inversion platform based on porous silicon nanoparticles for efficient cancer cell recognition and combination therapy. *ACS Appl Mater Interfaces*. 2017;9:10034–10046. doi:10.1021/acsami.7b02196
28. Mei L, Liu Y, Xia C, Zhou Y, Zhang Z, He Q. Polymer-drug nanoparticles combine doxorubicin carrier and heparin bioactivity functionalities for primary and metastatic cancer treatment. *Mol Pharm*. 2017;14:513–522. doi:10.1021/acs.molpharmaceut.6b00979
29. Chen Y, Yue Q, De G, et al. Inhibition of breast cancer metastasis by paclitaxel-loaded pH responsive poly (β-amino ester) copolymer micelles. *Nanomedicine*. 2017;12:147–164. doi:10.2217/nnm-2016-0335
30. Ravar F, Saadat E, Gholami M, et al. Hyaluronic acid-coated liposomes for targeted delivery of paclitaxel, in-vitro characterization and in-vivo evaluation. *J Control Release*. 2016;229:10–22. doi:10.1016/j.jconrel.2016.03.012
31. Li J, Huo M, Wang J, et al. Redox-sensitive micelles self-assembled from amphiphilic hyaluronic acid-deoxycholic acid conjugates for targeted intracellular delivery of paclitaxel. *Biomaterials*. 2012;33:2310–2320. doi:10.1016/j.biomaterials.2011.11.022
32. Li H, Zhang P, Luo J, et al. Chondroitin sulfate-linked prodrug nanoparticles target the Golgi apparatus for cancer metastasis treatment. *ACS Nano*. 2019;13:9386–9396. doi:10.1021/acsnano.9b04166

33. Chen X, Chen J, Li B, et al. PLGA-PEG-PLGA triblock copolymeric micelles as oral drug delivery system: in vitro drug release and in vivo pharmacokinetics assessment. *J Colloid Interface Sci*. 2017;490:542–552.
34. Cai D, Gao W, He B, et al. Hydrophobic penetrating peptide PFVYLI-modified stealth liposomes for doxorubicin delivery in breast cancer therapy. *Biomaterials*. 2014;35:2283–2294. doi:10.1016/j.biomaterials.2013.11.088
35. Xu W, Siddiqui IA, Nihal M, et al. Aptamer-conjugated and doxorubicin-loaded unimolecular micelles for targeted therapy of prostate cancer. *Biomaterials*. 2013;34(21):5244–5253. doi:10.1016/j.biomaterials.2013.03.006
36. Zavvar T, Babaei M, Abnous K, et al. Synthesis of multimodal polymersomes for targeted drug delivery and MR/fluorescence imaging in metastatic breast cancer model. *Int J Pharm*. 2020;578:119091.
37. Zhang XQ, Huang YM, Song HL, et al. Inhibition of growth and lung metastasis of breast cancer by tumor-homing triple-bioresponsive nanotherapeutics. *J Control Release*. 2020;328:454–469.
38. Dancy JG, Wadajkar AS, Connolly NP, et al. Decreased nonspecific adhesivity, receptor-targeted therapeutic nanoparticles for primary and metastatic breast cancer. *Sci Adv*. 2020;6:eaax3931.
39. Yu S, Ding J, He C, Cao Y, Xu W, Chen X. Disulfide cross-linked polyurethane micelles as a reduction-triggered drug delivery system for cancer therapy. *Adv Healthcare Mater*. 2014;3:752–760.
40. Chen W, Zhong P, Meng F, et al. Redox and pH-responsive degradable micelles for dually activated intracellular anticancer drug release. *J Control Release*. 2013;169:171–179.
41. Pachmayr E, Treese C, Stein U. Underlying mechanisms for distant metastasis - Molecular biology. *Visc Med*. 2017;33:11–20.
42. Rosenberg JE, Bambury RM, Van Allen EM, et al. A Phase II trial of AS1411 (a novel nucleolin-targeted DNA aptamer) in metastatic renal cell carcinoma. *Invest New Drugs*. 2014;32:178–187.
43. Sun H, Meng Q, Tang S, et al. Inhibition of breast cancer metastasis by pluronic copolymers with moderate hydrophilic-lipophilic balance. *Mol Pharm*. 2015;12:3323–3331.
44. Jiang K, Song X, Yang L, et al. Enhanced antitumor and anti-metastasis efficacy against aggressive breast cancer with a fibronectin-targeting liposomal doxorubicin. *J Control Release*. 2018;271:21–30.
45. Torchilin V. Tumor delivery of macromolecular drugs based on the EPR effect. *Adv Drug Deliv Rev*. 2011;63:131–135.

International Journal of Nanomedicine Dovepress

Publish your work in this journal

The International Journal of Nanomedicine is an international, peer-reviewed journal focusing on the application of nanotechnology in diagnostics, therapeutics, and drug delivery systems throughout the biomedical field. This journal is indexed on PubMed Central, MedLine, CAS, SciSearch®, Current Contents®/Clinical Medicine, Journal Citation Reports/Science Edition, EMBase, Scopus and the Elsevier Bibliographic databases. The manuscript management system is completely online and includes a very quick and fair peer-review system, which is all easy to use. Visit http://www.dovepress.com/testimonials.php to read real quotes from published authors.

Submit your manuscript here: https://www.dovepress.com/international-journal-of-nanomedicine-journal